ALICE/99-41
Internal Note/DIM
September 06, 1999

Stations 4 and 5 of the ALICE Muon Spectrometer: Modular Approach.

V. Gertsenstein, B. Komkov, V. Kozlov, D. Markushin, N. Miftakhov,
V. Nikulin, V. Samsonov, O. Tarasenkova, and S. Volkov
Presented by A. Vorobyov at the tracking group meeting at CERN, May 4-5.
PNPI, Gatchina

Introduction

Here we present a modular approach for the tracking chambers **TC7, TC8** (station 4) and, **TC9, TC10** (station 5) of the ALICE Muon spectrometer (notations from the ALICE muon spectrometer Technical Proposal [1]). The chambers are located between the dipole magnet and the iron wall of the muon shield.

This approach renews our proposal formulated first in 1996 [2] and also takes into account the results of the beam tests of the one square meter SCSC (Segmented Cathode Strip Chamber) prototype designed and constructed at PNPI [3].

The general requirements and segmentation criteria are presented in Section 1. Some details of the chamber design are given in Section 2. Section 3 describes the technology of the chamber construction. The results of the `ANSYS` calculation of the cathode planes possible deformations are presented in Section 4. The primary consideration of the chariot design could be found in Section 5.

1 Segmentation.

The central $Pb-Pb$ collision at LHC energies results in high multiplicity in the tracking chambers even behind a more than 4 meters long absorber. The number of hits at the rear chambers is expected to be around $N \sim 400-500$ per collision.

The resolution of the ALICE muon spectrometer in effective mass should be sufficient to distinguish between Υ, Υ', and Υ''. Hence the required spatial resolution for tracking system should be 70–100 microns in the vertical plane. The tracker elements should not significantly deteriorate the particle direction due to multiple scattering, i.e. the thickness of one chamber should not exceed 3%.

The dimensions of the stations 4 and 5 are presented in Table 1. This area will be covered with SCSC

Parameter	Station 4	Station 5
External sensitive zone radius (cm)	221	257
Internal sensitive zone radius (cm)	43	50
Anode-cathode gap (mm)	2.5	2.5
Anode wire diameter (μm)	25	25
Anode wire spacing (mm)	2.5	2.5

Table 1: Main parameters of the tracking chambers TC7-TC10

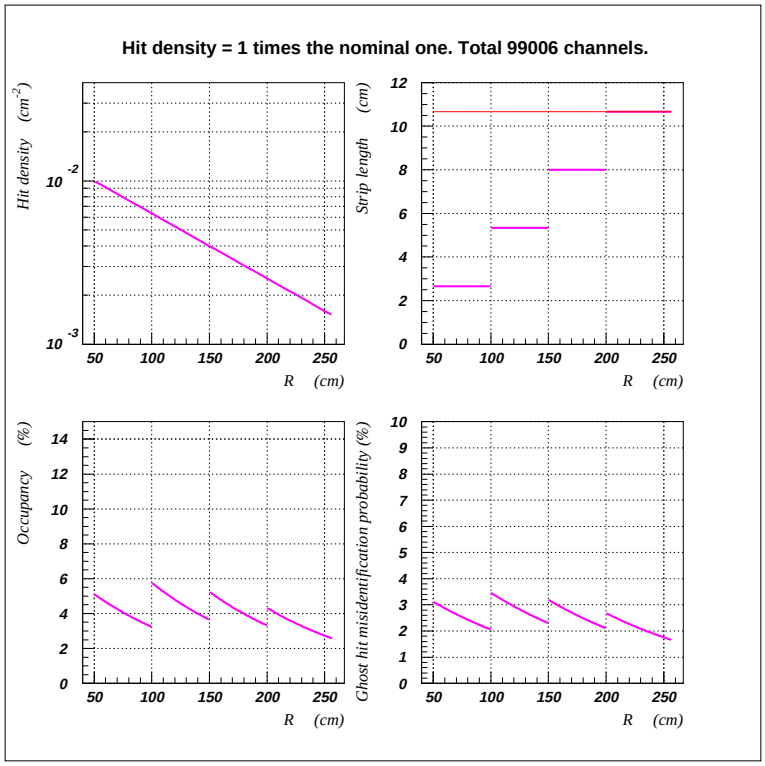

Figure 1: Hit density, segmentation, and occupancy in the bending plane, and the probability to attribute the ghost hit as real one for station 5 calculated for the new reference hit density in open geometry.

with the geometry parameters shown in Table 1. Both cathode planes contain strips of 5 mm width. In one cathode plane the strips are perpendicular to the anode wires direction (bending plane), in the other, the strips are parallel to the anode wires direction (non-bending plane).

In order to achieve the required spatial resolution in the bending plane it is necessary to minimize the influence of the background hits. Quantitatively this results in limitation in the *occupancy*[1]: it should not exceed 5%. The strip length in the bending plane has been estimated from this condition.

The strip length in the non-bending plane was chosen in a different way. The 2-track resolution of the SCSC is demonstrated to be below 0.7 mm [5, 6], thus one can easily distinguish the firing of **each** individual wire located at the distance of 2.5 mm. That is why for the non-bending plane the granularity should be chosen taking into account not the occupancy of the separate strip but the probability of the ghost hits in the area determined as $L_X \times L_Y$, where L_X and L_Y are the length of the strips in the non-bending and bending planes, respectively. The details could be found in the ALICE note [7].

The calculations were performed using the particle density given by Andreas Morsch [8]: it changes exponentially from $n = 1.5 \times 10^{-3}\ cm^{-2}$ at 9° to $n = 10^{-2}\ cm^{-2}$ at 2°. The results for station 5 are presented in Figure 1. Similar results are obtained for station 4.

The proposed segmentation is illustrated by Figure 1 (upper right plot) and Figure 2. The strip length in the bending plane grows from 2.6 cm in the center up to 10.66 cm in the peripheric area. This segmentation keeps the occupancy of the bending plane cathode at an affordable level ensuring the required resolution. The non-bending plane cathodes are segmented in 10.66 cm strips over the whole area. With such segmentation, the probability to find a ghost hit (in addition to the physical hit) could reach 25 %. The correlation of charges induced onto the opposite cathodes could be used to reject the ghost hits. As these charges are not perfectly equal (the dispersion of their ratio is about 15%), there is a non-negligible probability of confusing the ghost hit with a real one. In this case the tracking information from the given chamber will be lost. This probability, calculated using the experimentally measured

[1]By occupancy in the bending plane we understand the probability to find a hit in a cluster of neighboring strips.

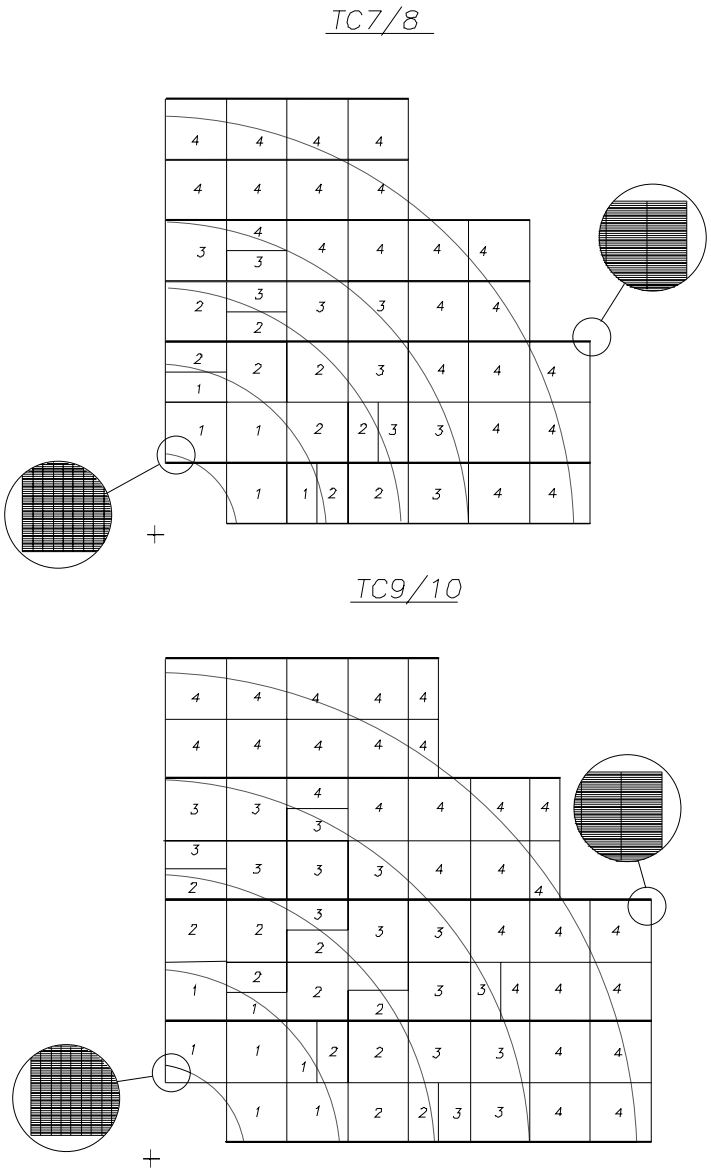

Figure 2: Actual segmentation in the bending plane. Each square represents an individual PCB, forming the cathode. Numbers in squares correspond to different strip length values: 1 → 2.66 cm, 2 → 5.33 cm, 3 → 8.0 cm and 4 → 10.66 cm. Note the possibility to use the chamber design for TC9/10 also for chambers TC7/8. The thick lines correspond to the module edges.

Zone	Parameter	TC7/8	TC9/10
Bending plane			
Zone 1	R_{in} (cm)	43	50
	R_{out} (cm)	90	100
L_{strip}=26.6 mm	N_{MCM}	192	276
Zone 2	R_{in} (cm)	90	100
	R_{out} (cm)	130	150
L_{strip}=53.3 mm	N_{MCM}	144	192
Zone 3	R_{in} (cm)	130	150
	R_{out} (cm)	165	200
L_{strip}=80.0 mm	N_{MCM}	112	224
Zone 4	R_{in} (cm)	165	200
	R_{out} (cm)	261	257
L_{strip}=106.6 mm	N_{MCM}	156	232
Total	N_{MCM}	604	936
	N_{strip}	38,656	59,904
Non-bending plane	R_{in} (cm)	43.	50.
	R_{out} (cm)	221.	257.
L_{strip} 106.6 mm	N_{MCM}	416	552
	N_{strip}	26,624	35,328
Total	N_{MCM}	**1,020**	**1,488**
	N_{strip}	**65,280**	**95,232**

Table 2: Segmentation of the Tracking Chambers TC7-TC10

induced charge correlation, is shown in the low right part of Figure 1.

The cathode will be formed of the Printed Circuit Boards (PCBs) of $32\times32cm^2$ size with 64 sequential strips across the strip direction. In this case the usage of 64-channel MCM-64 front end electronics cards becomes quite natural. The distribution of the PCBs with different strip length over the sensitive area of the chambers in the bending plane is shown in Figure 2. For the non-bending plane a uniform strip length of 10.66 cm has been chosen. The number of channels resulting from the proposed segmentation is presented in Table 2. These numbers slightly differ from the estimations [7] because the real segmentation due to the fact that the PCB with a given granularity differs from the ideal one used in [7].

The resulting numbers of channels are greater than estimated in the TP: 65 thousands vs 60 thousands for TC7/8 and 95 thousands vs 86 thousands for TC9/10. The difference is caused mainly by the additional requirement to keep the ghost hit probability at a low level.

That is, roughly speaking, the fully equipped station 4 requires 2000 MCM-64 cards, station 5 — 3000. Another 500 MCM-64 cards should be produced as spares.

2 Chamber Design

2.1 General design.

Each chamber plane will consist of several modules fixed horizontally in the ladder style on the external frame with overlapping at the edges (see Figure 3). Each module height (sensitive area) is 64 cm, its length depends on its position and could vary from 120 cm to 260 cm. The overlap zone will be 22 mm: 2×5 mm for anode spacers, 2×5 mm for dead zones (since the neighboring strip, required for the position reconstruction, is missing) and 2 mm for safe detection of the inclined track.

The modules are fixed on the frames only, all fixation is outside of the acceptance of the spectrometer.

Due to axial symmetry of the particle distribution one needs to produce only 4 types of modules per station, 8 modules of each type[2].

[2]Note that in the option when station 4 and 5 are identical, only 4 types of modules will be needed for two stations, 16

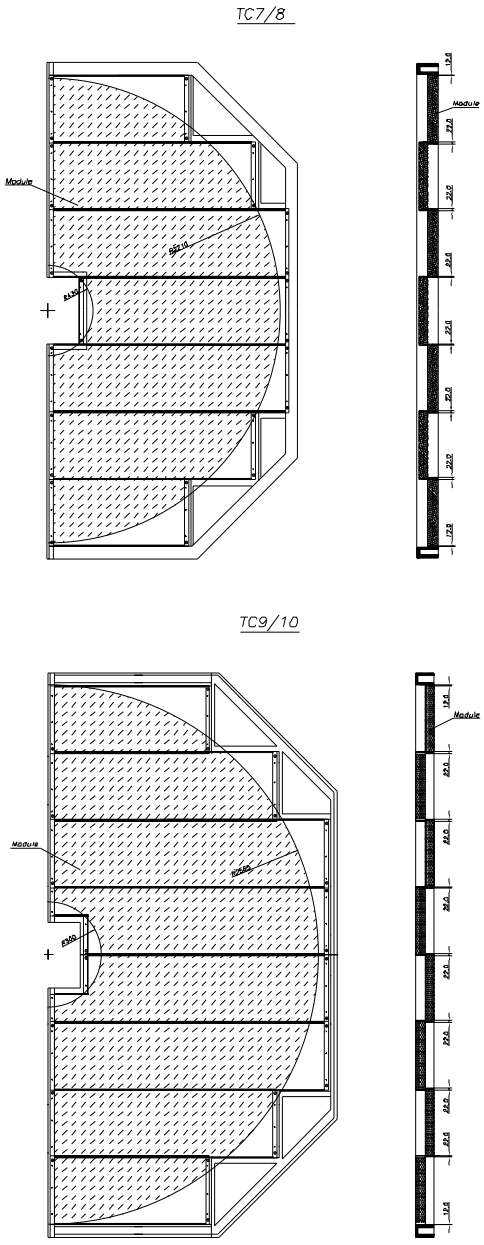

Figure 3: Modules fixation on the chamber frame. Shaded area denotes to the spectrometer acceptance zone.

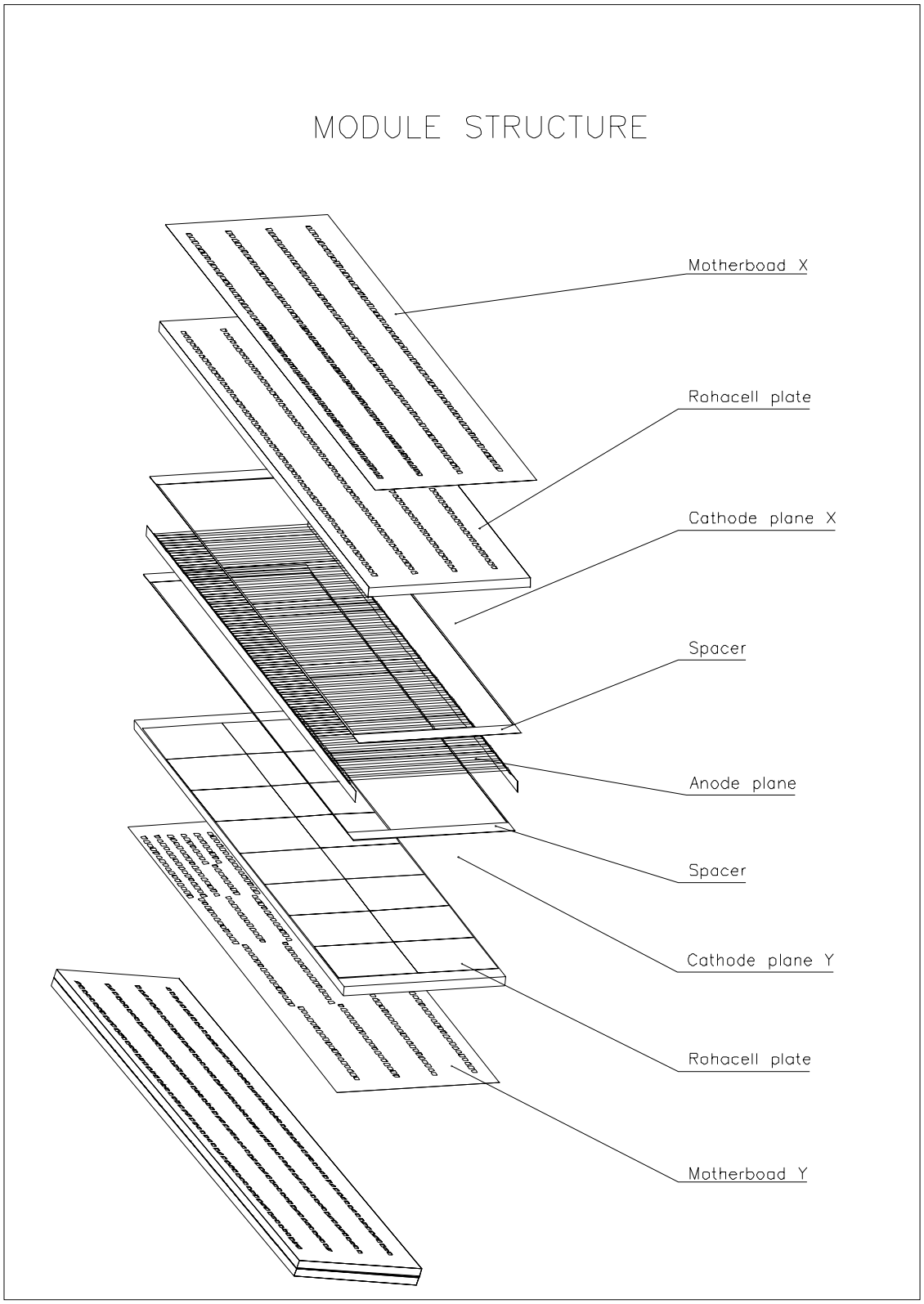

Figure 4: Exploded view of the module. Assembled module is shown at bottom.

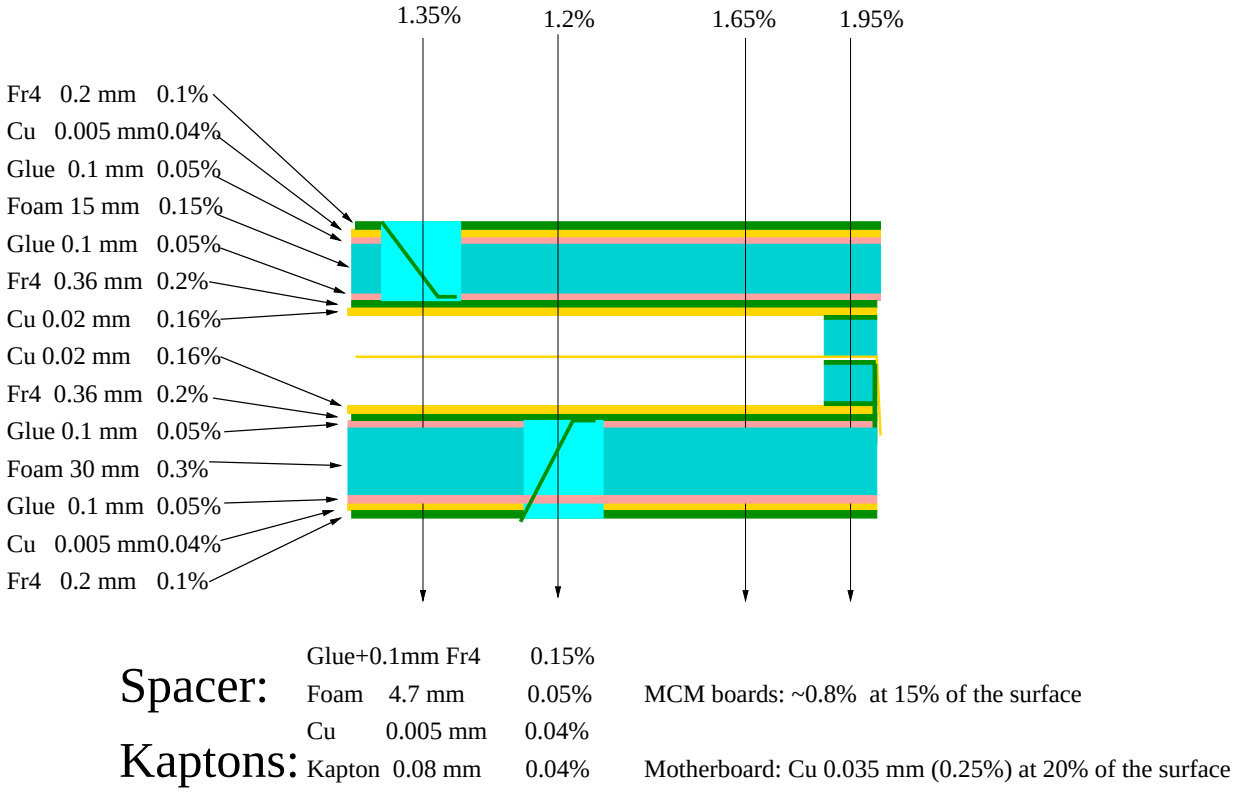

Figure 5: The contribution to the thickness of the chamber (in X/X_0) from the various components.

The internal structure of the chamber is shown in Figure 4. The cathode sandwich consists of a foam layer with the cathode plate glued on one side and the motherboard glued on the other. The foam and the motherboard have holes in order to connect cathode pads to the read-out electronics. The anode wires will be tensioned on the cathode which measures coordinates in the non-bending plane: as all strips have the same length, it has a homogeneous hole pattern. A safe conservative value of 30 mm was taken for the thickness of the foam layer. The anode spacers are made of Rohacell foam. The spacers which are glued on the non-bending cathode have a wire support made of 0.1 mm thick plastic. The wires are bonded to the anode card glued to the back edge of the cathode. We choose the thickness of 15 mm for the foam layer of the opposite cathode. The thickness of the foam layers is not yet optimized and could possibly be reduced.

The spacer at the other side (close to the bending – Y – plane cathode) is not continuous, it is glued in few points only. The remaining slit is 2.5 mm wide, it is expected to cover more than 95 % of the long sides of the module. This slit would enable to repair the majority of the wires if needed. The edge of the chamber could be covered with a transparent film which might be useful during the tests of the chamber to observe possible discharges.

2.2 Materials and Thickness Estimates.

According to our experience the reliable way to produce a good quality cathode surface is to use the cathode PCBs with a thickness of 0.36 mm or more. The motherboard PCB thickness could be as low as 0.2 mm: it should be chosen for sandwich stiffness considerations.

The motherboard should have a copper layer at the backside which serves as an electric screen. Its thickness could be as low as 5 microns. The front side of the motherboard contains a circuit which connects the MCMs with the low voltage power supply, provides required control signals and extracts

modules of each type.

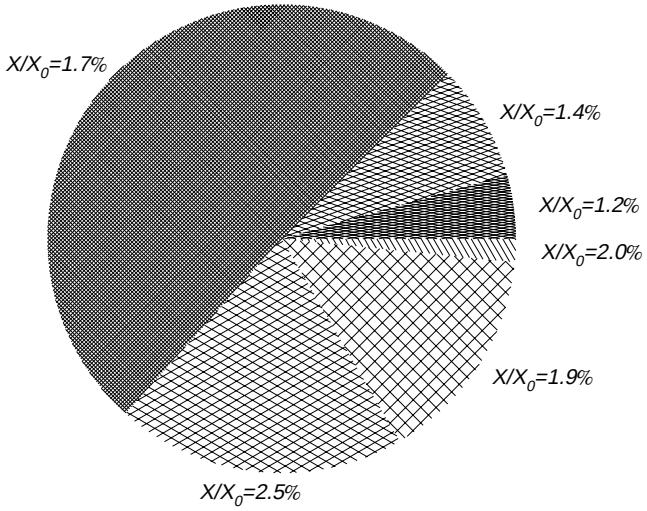

Figure 6: The material budget of the chamber (average percentage of the total area).

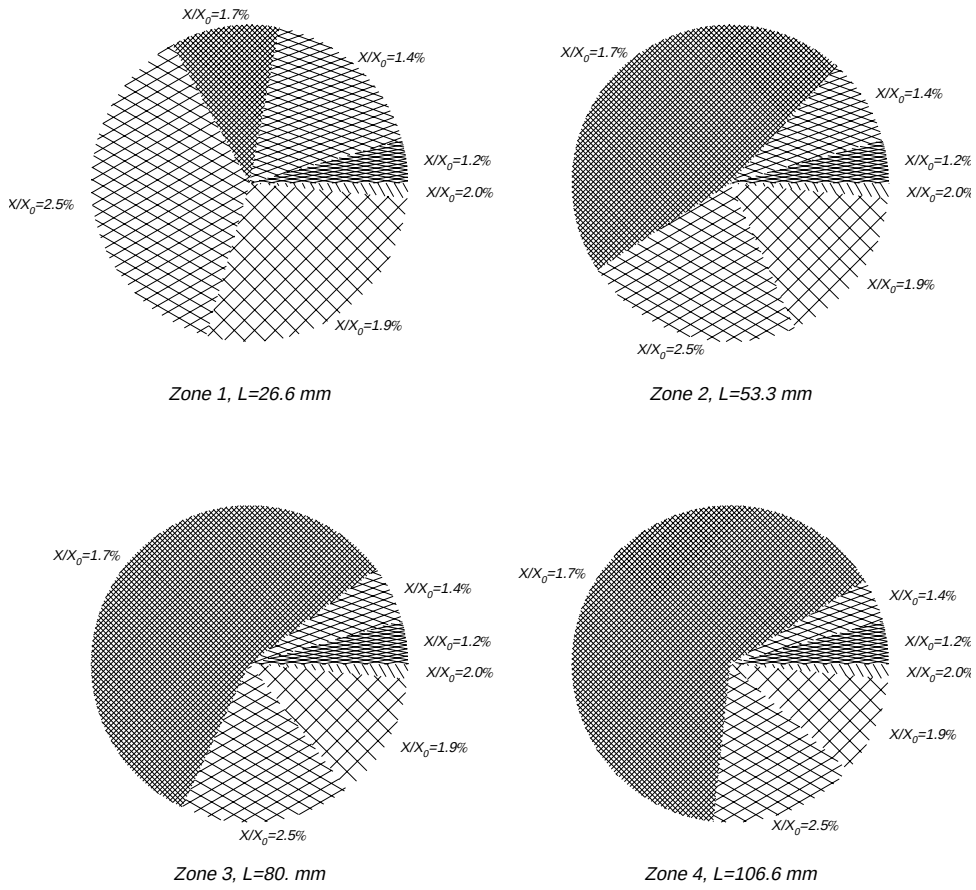

Figure 7: The material budget of the chamber in different segmentation zones.

MCM output data. As MCMs consume substantial power, we plan to use a thick (0.35 mm) layer of copper. We expect that about 10 % of each motherboard surface will be covered with this copper.

We expect that the copper layer at the cathode PCB will be around 20 microns (5 microns initially, plus 15 microns added during hole metallization in the standard industrial procedure).

The epoxy glue gives a non-negligible contribution to the thickness and should be also taken into account. According to our experience a 100 micron glue layer is required to maintain a reliable mechanical contact between the foam and the PCB skins.

The thickness of the kapton cable lead, to transmit signals from the cathode to the motherboard, is estimated to be 0.1 % X_0.

The estimated contributions of various chamber constituents to the thickness are shown in Figure 5. Figure 6 illustrates the fractions of the total area of the chamber with given radiation length. Same distributions for the four segmentations are shown in Figure 7 and in Table 3.

The maximal chamber thickness will be in the module overlap zone: $X/X_0 \simeq 3.7$ % in the spacer zone

	Zone 1 L=26.6mm	Zone 2 L=53.3mm	Zone 3 L=80mm	Zone 4 L=106.6mm	Mean
Holes in sandwich X ($X/X_0 = 1.2\%$)	4.4%	4.4%	4.4%	4.4%	4.4%
Holes in sandwich Y ($X/X_0 = 1.4\%$)	17.6%	8.8%	5.8%	4.4%	8%
Pure sandwich ($X/X_0 = 1.7\%$)	11.1%	46.0%	57.8%	64.5%	51.1%
Sandwich + Cu from MB ($X/X_0 = 1.9\%$)	37.5%	22.5%	17.5%	15.0%	20%
Sandwich + MCM ($X/X_0 = 2.5\%$)	27.9%	16.8%	13.0%	10.2%	15%
Sandwich + spacers ($X/X_0 = 2.0\%$)	1.5%	1.5%	1.5%	1.5%	1.5%

Table 3: Fractions of the module surface with certain thickness for different segmentations.

(~ 1.5 % of the total area) and $X/X_0 \simeq 3.4$ % in the sandwich overlap zone (~ 3 % of the total area).

To that one should add the contribution of the anode wires ($\sim 0.6\%X_0$ filling 0.8% of the sensitive area), the anode PCB ($\sim 15\%X_0$ filling 0.09% of the sensitive area) and the bonding material. The contribution of the last item could substantially vary depending on the bonding method chosen. The conservative estimation (soldering with tin, each contact is 1 mm^2 of area and 0.3 mm thick) results in an additional thickness of about $3\%X_0$ at 2%, 1.5%, 1.1% and 0.9% of the total area in zones 1, 2, 3, and 4 correspondingly.

2.3 Gas Gain.

The results presented below are obtained for the chamber with an anode-cathode separation of 2.5 mm, anode wires spacing of 2.5 mm and anode wire diameter of 25 microns. The chamber is filled with a 70% Ar + 30% CO_2 gas mixture.

For the gas gain (G) estimates we fit the experimental data of Armitage et al. [10] to a function

$$\ln G = \frac{Aq}{b} \exp(-\frac{B}{E_a}),$$

where $E_a = 4q/d$ is the electric field at the wire surface, q is the charge per 1 meter of the wire (measured in volts; 1 V = $2\pi\varepsilon_0$ C/m), and d is the anode wire diameter. The fit resulted in the parameters $A = 5.7953 \times 10^{-2}$ and $B = 1.2295 \times 10^5$.

The value of q is determined by the chamber geometry:

$$q = \frac{V}{\frac{\pi a}{s} - \ln \frac{\pi d}{s}},$$

where a is the anode-cathode separation, and s is the wire spacing.

The influence of the anode-cathode gap size variations and displacement of the wire on the gas gain are presented in Figure 8. One can see that we can afford up to 100 micron variation in the anode-cathode distance and up to 200 micron in displacements of the anode wire position.

The critical mechanical tension of the anode wires to avoid the transverse non-stability is given by the formula [9]:

$$T_c = \pi\varepsilon_0(\frac{qL}{s})^2,$$

where L is the length of the wire, the permittivity of free space $\varepsilon_0 \simeq 8.8542 \times 10^{-12}$ F/m. For the case $L = 64$ cm, $s = 2.5$ mm and $q = 325$ V (corresponds to $HV = 2150$ V) $T_c = 0.193$ N$\simeq 20$ g. We suggest to use wires of 25 microns in diameter. These wires proved to be reliable in assembling of the chamber and in operation. We choose 40 grammes as the nominal wire tension, which is well below the elasticity limit[3].

As one can see from Figure 9 each 5 micron change in the anode wire diameter results in an ~ 80 V change in high voltage to keep the gas gain at the same level.

[3]We suggest to use the tungsten-rhenium (3%) wire from *Orsam Sylvania Inc.*, which has an elasticity limit of 140 grammes

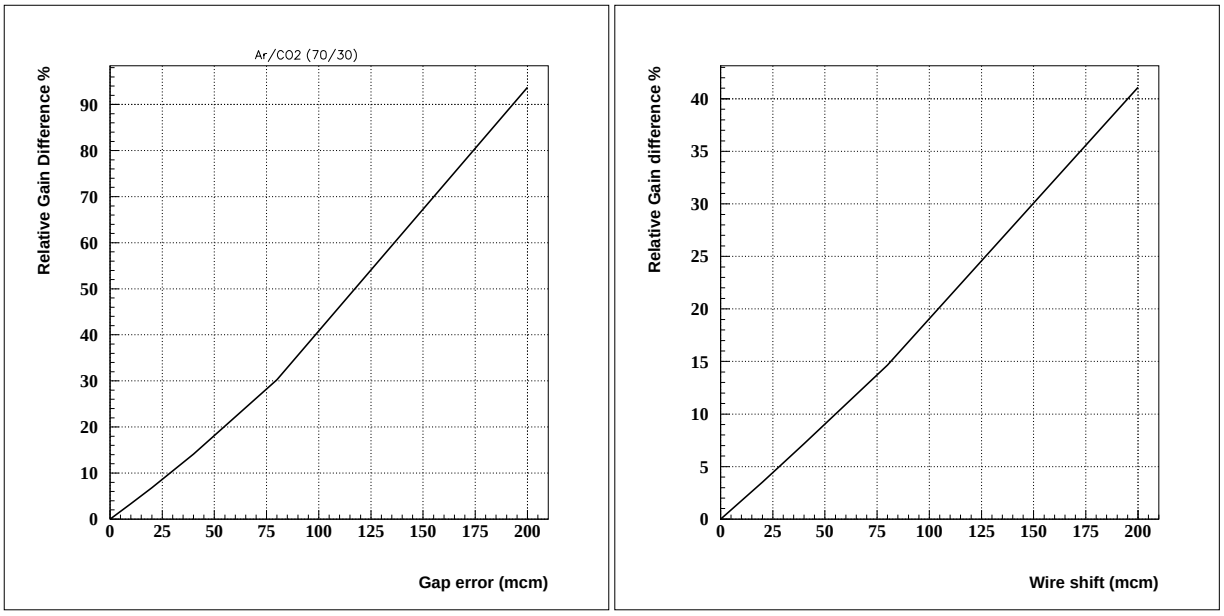

Figure 8: Influence of the variations in the anode-cathode distance (right plot) and the wire displacement on gas gain.

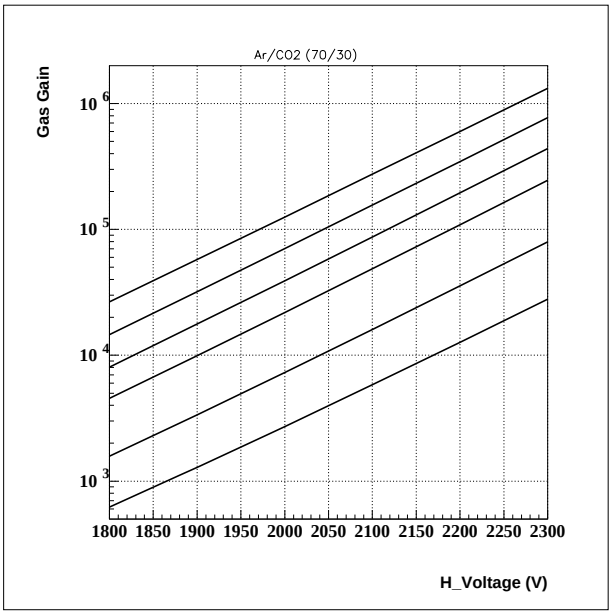

Figure 9: Gas gain dependence on high voltage for various diameters of the anode wire: 15 (the top curve), 20, 25, 30, 40 and 50 (the bottom curve) microns.

3 Technology Review.

3.1 PCB Alignment Equipment.

The alignment procedure for the cathode PCBs will take place on a special flat iron table equipped with a high precision optical system and a moving platform. The following operations will be performed:

- Measurement of the position of each pad on the cathode PCB with respect to the reference marks before gluing;
- Alignment of the PCBs during the gluing process;
- Measurement of the pad alignment precision for the glued cathode;
- Measurement of the external optical mark position with respect to the PCB reference marks;
- Measurement of the individual wire positions.

The gluing should be done when the PCBs are positioned on the flat table in a way that the strips from the neighboring boards are parallel and equidistant.

In order to accomplish this task, the boards will have high precision reference marks in the corners on both sides of the board. The marks are actually narrow ($\sim 100\ \mu m$) slits in the strips at well defined positions and crosses on the other side. Each PCB is inserted between two CCD cameras so that the relative position of the component side reference mark with respect to the strip side mark could be measured with high precision (~ 10 microns). The CCD devices could be calibrated before by inserting of a thin glass layer with a reference mark on it.

The procedure is illustrated in Figures 10 and 11.

The PCB alignment system consists of:

- The assembling table (size $3.0 \times 1.0 m^2$, flatness better than 50 μm), where all phases of the alignment and gluing are done. The table is equipped with a linear accurator with a timing belt drive for moving the PCB displacement unit above the table and an optical unit, which links the global frame with the PCB displacement unit frame. It consists of:
  - 2 CCD lines fixed to an appropriate linear accurator (X or Y);
  - 2 CCD lines fixed to the PCB displacement unit;
  - A semiconductor laser for illumination of the CCD line.
- PCB displacement unit, which can move in both directions; the unit contains the following equipment:
  - Vacuum clamping system to handle PCBs (cathode and motherboards).
  - Optical head with 4 CCD matrix, 2 CCD lines and the reference mark illumination system. All elements are rigidly fixed onto the optical head and define the local frame (X', Y').
  - High precision rotation of the PCB displacement unit.
  - Vertical displacement system (precision $\simeq 100\ \mu m$).
  - 3 probes to verify the planarity and to measure the vertical displacement of the displacement unit.
  - Removable equipment for gluing of the PCBs (not shown).

The local frame is defined with 4 CCD matrix as shown in Figure 10. The CCD cameras 1,2,3 measure the position of the PCB cathode element in the local frame. The CCD camera 4 checks the PCB position with respect to the neighboring element. Two CCD lines together with a semiconductor laser are fixed on a table and define the X axis. The laser ray passes through the CCD lines fixed on the displacement unit providing the angular and the coordinate (Y) information. The position in X is defined by the linear accurator using an encoder with a finder system.

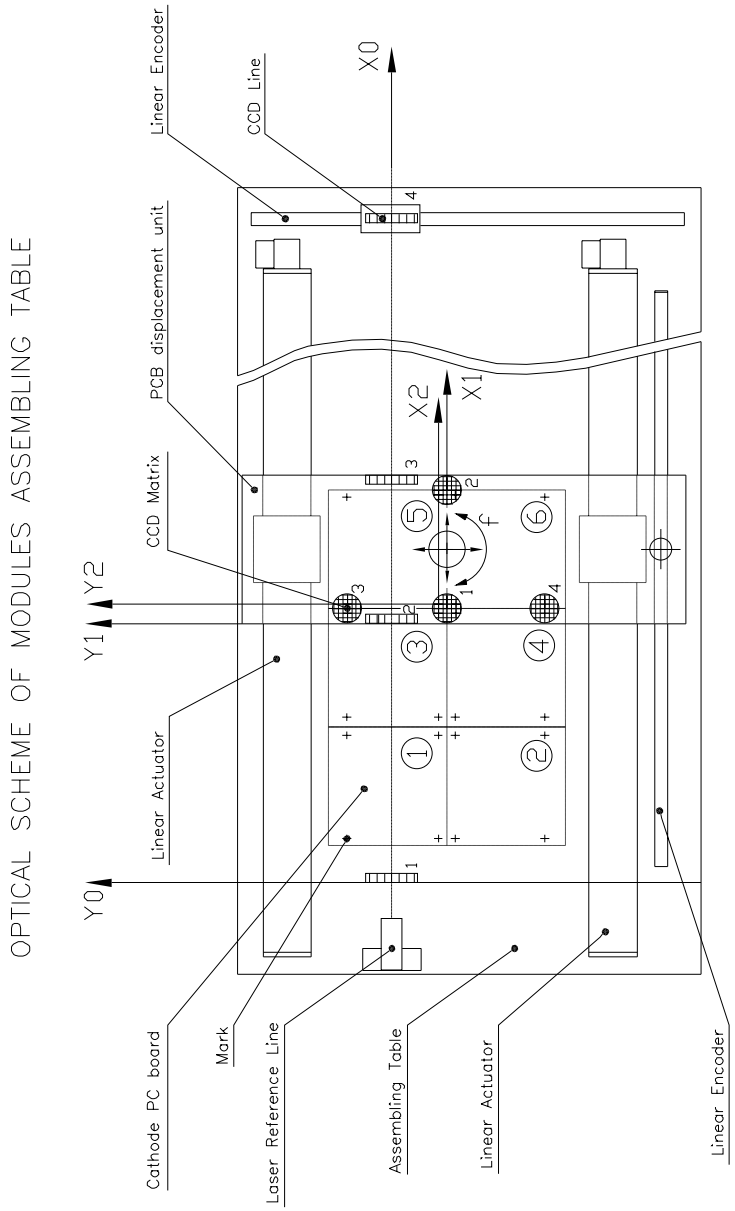

Figure 10: The PCB alignment table, optical schema.

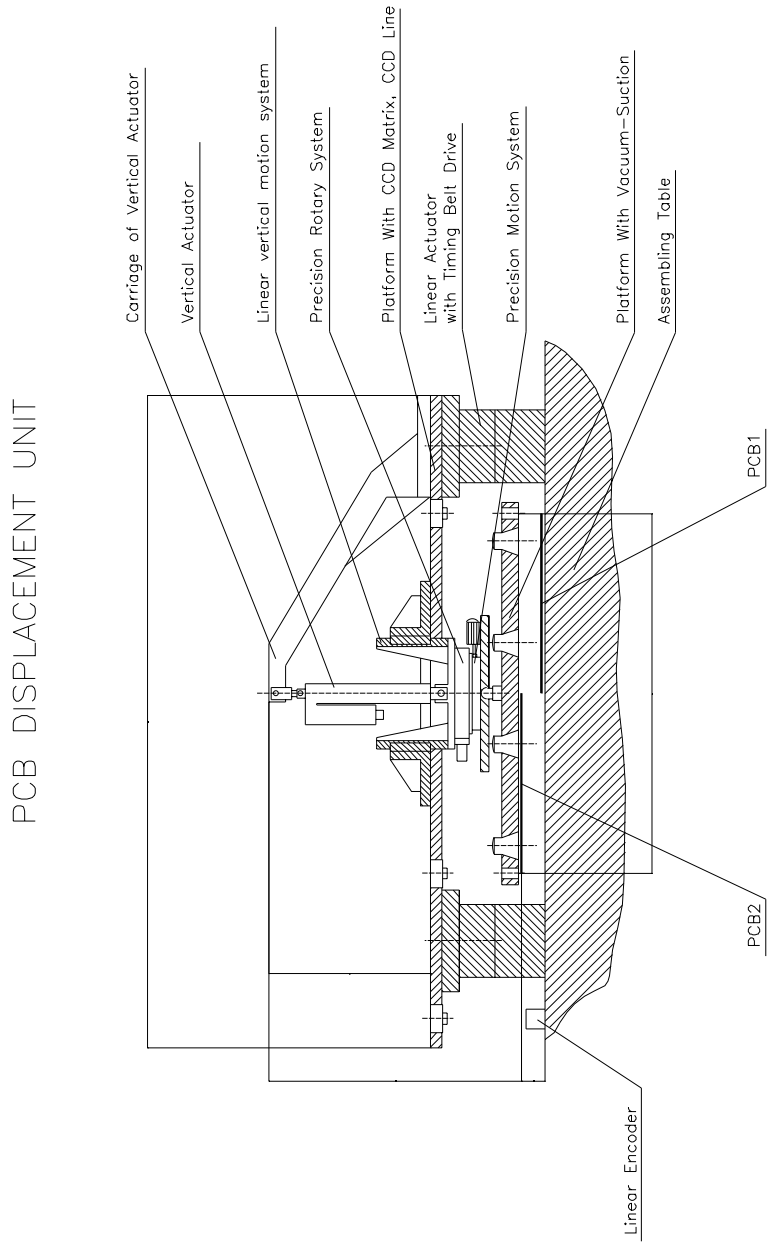

Figure 11: The PCB displacement unit. Note that the distance between the table surface and PCB fixed in displacement unit is exaggerated: in reality all movements will be done just above the table surface in order to keep the focal distance of the CCD cameras unchanged.

After finishing the gluing cathode sandwich procedure, it should be turned with the pad side up. Then a thin wire would be fixed along the gap between strips and the CCD camera would move along it, storing in a computer data base the deviation of the strip position from the wire.

Using the same wire one can measure the position of the external glass reference mark (Figure 12) with respect to the internal marks. These marks (3 per module) would serve for determination of the absolute module position. According to our estimates, the position of each pad with respect of the external optical marks will be known with a precision of about 20 microns.

The high precision checking balls are used to align the modules (see Figure 12). The balls could be inserted into the optical mark support with a precision of 2 — 3 microns. The absolute positions of each module will be measured using the parallax method (one of the possible options is presented in Figure 13). If the precision of angular measurements is about one angular second and the base (distance between the two positions of the angular measurement devices) is 1 meter ± 5 microns, the expected absolute alignment precision is about 30 microns. The angular measurement devices could be located below the chamber as shown in the left part of Figure 13. The exact position of the device should be optimized in order to obtain the best precision.

3.2 Assembling.

The chamber would be assembled in the following sequence:

1. Checking the gas tightness of the individual cathode PCBs.
2. Bonding of the flat kapton cables to the cathode PCB.
3. Checking of the contacts between the cathode pads and the kaptons.
4. Successive strip-to-strip alignment of the cathode PCBs (see section 3.1) with temporary fixation of the PCBs with magnetized iron bars and immediate gluing of the new-aligned PCB with 0.1 mm thick plastic band.
5. Gluing of the Rohacell layer.
6. Gluing of the motherboard.
7. Bonding of the kapton cables to the motherboard.
8. Checking of the contacts between the cathode pads and the MCM connectors;
9. Gluing the anode spacers.
10. Winding and bonding the anode wires.
11. Verifying the anode wire positions at the assembling table. For this purpose the cathode sandwich with the anode wires will be placed onto the assembling table. The PCB displacement unit with CCD cameras will scan the surface, relative position of each wire could be easily measured with the precision of 10 microns on both sides of the chamber.
12. The wire tension measurement.
13. Final cleaning of the chamber elements.
14. Assembling of the chamber, preliminary high voltage tests and hermetization.

The test strips could be used for checking the contacts between the cathode pads and the MCM connectors. The absolute alignment should be done by means of the optical system using the precise reference marks on the frame of each module.

The wire tension is measured with standard equipment which has been already used at PNPI during construction of the PHENIX drift chamber.

The cut view of the module is shown in Figure 14. Note that the anode wires are bonded to the anode PCB glued to the back edge of the module. The anode circuit is split into groups (8 cm long),

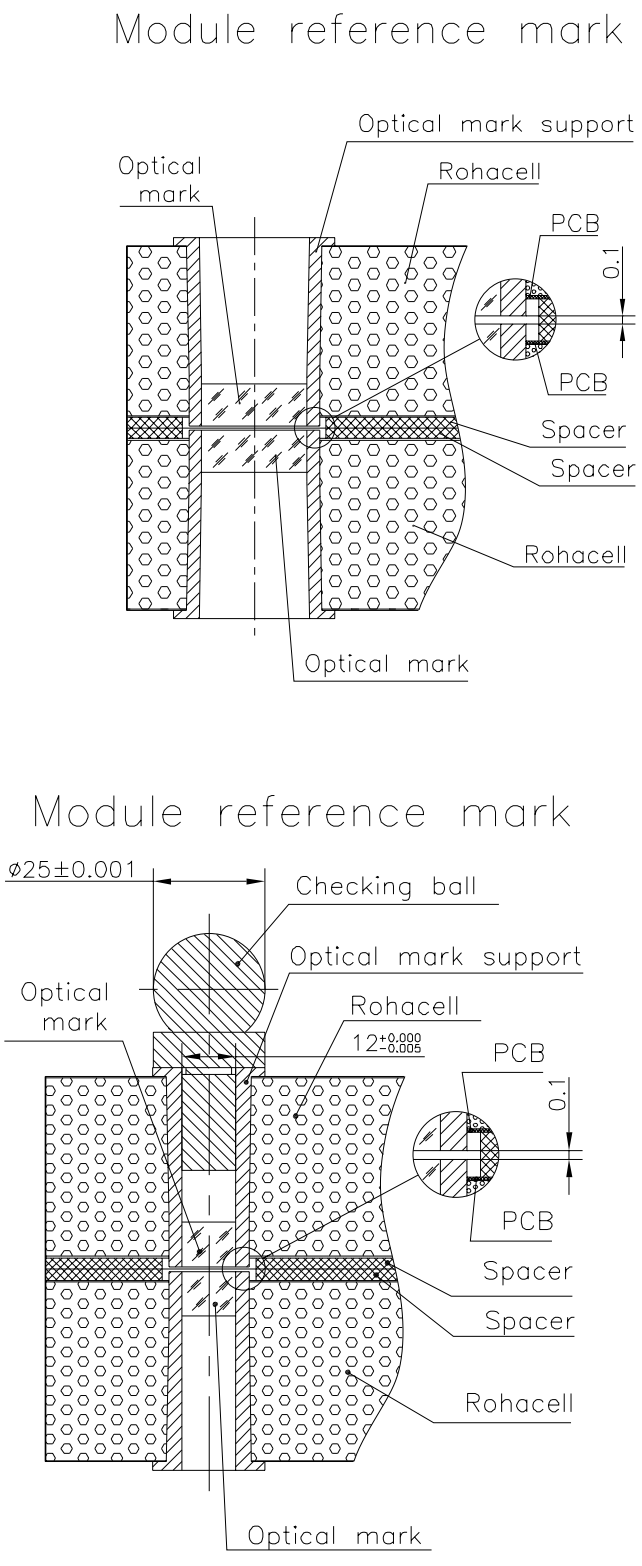

Figure 12: The cut view of the external reference mark without (upper part) and with (lower part) checking ball inserted.

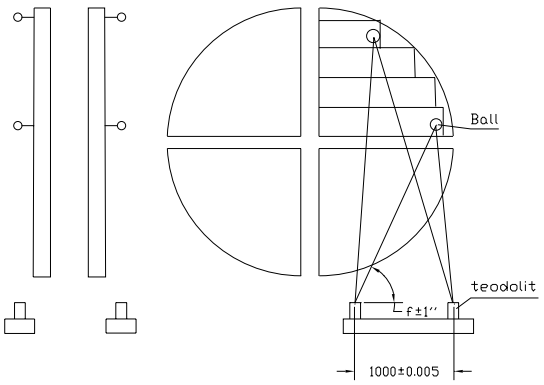

Figure 13: Schematic drawing of the absolute module position measurement using the parallax method.

each of them having an individual high voltage channel and an excessive current detection system. The appropriate electronics is located in a special hole in the foam near the edge of the chamber. The excessive current detector can indicate the defective section, allowing to decrease the voltage on this section.

3.3 Assembling Site at PNPI.

PNPI owns a stand-alone building with a hall of 200 m^2. The ceiling of the hall is 7 meter high and is equipped with a 5 tons crane.

The horizontal and vertical sizes of the hall are suitable for assembling and testing the tracking chambers for the ALICE muon spectrometer. A flat table for the chamber assembling is available with the flat area size of $3,000 \times 1,200$ mm^2. Also there is some standard equipment used for assembling and testing the wire chambers. In particular, there will be available an anode wire winding machine, a cosmic muon test station, a wire tension measuring system. The following equipment is not yet available:

- The flat table equipment (PCB displacement unit, optical and moving systems).
- A slab to press the cathode during gluing.
- A mechanism for the slab displacement.
- Clean zone.

3.4 Cooperation with industry.

We plan to use the industrial technology for the production of the cathode PCBs. First negotiations with several companies in St-Petersburg showed that they could produce the cathode PCBs according to our design with the size of 32×32 cm^2. The fabrication cost will be around 2.5 CHF per 1 dm^2. We are investigating also the possibility to produce the PCBs of larger sizes.

4 First results of the finite element analysis: the cathode plane deformations.

The cathode plane is a sandwich glued of the cathode PCBs, a layer of the Rohacell foam and the motherboards. The Rohacell and the motherboard have holes in order to enable the passage of the flat

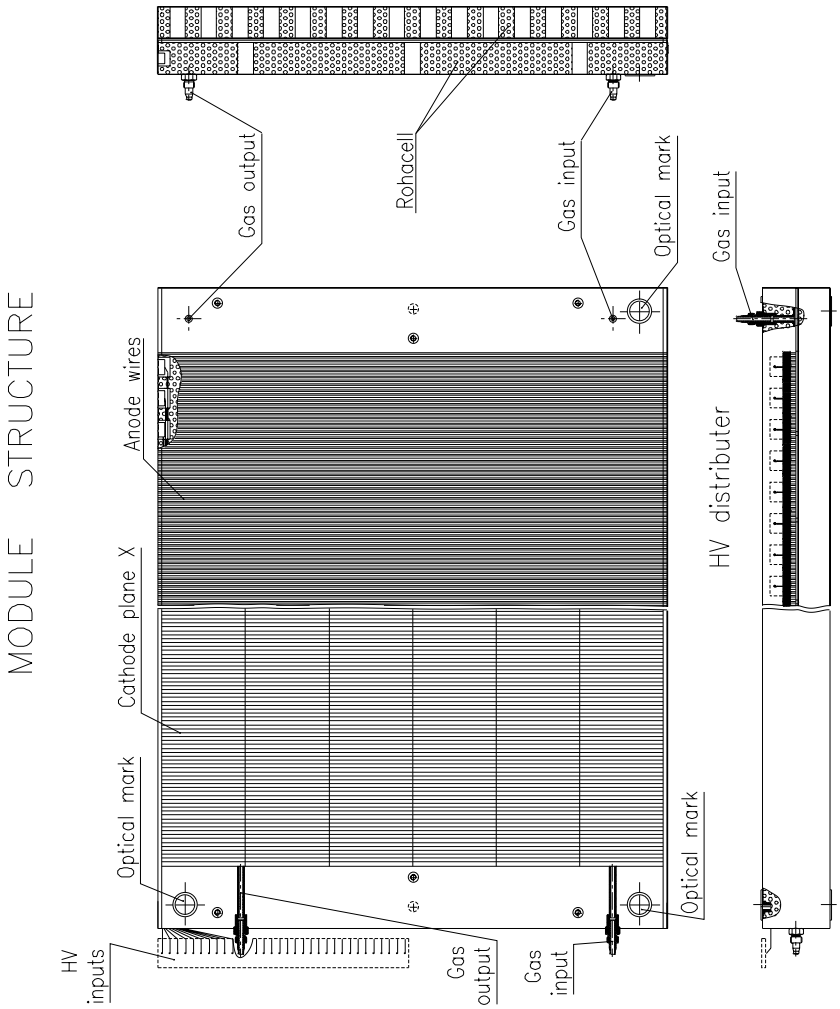

Figure 14: The cut view of the module.

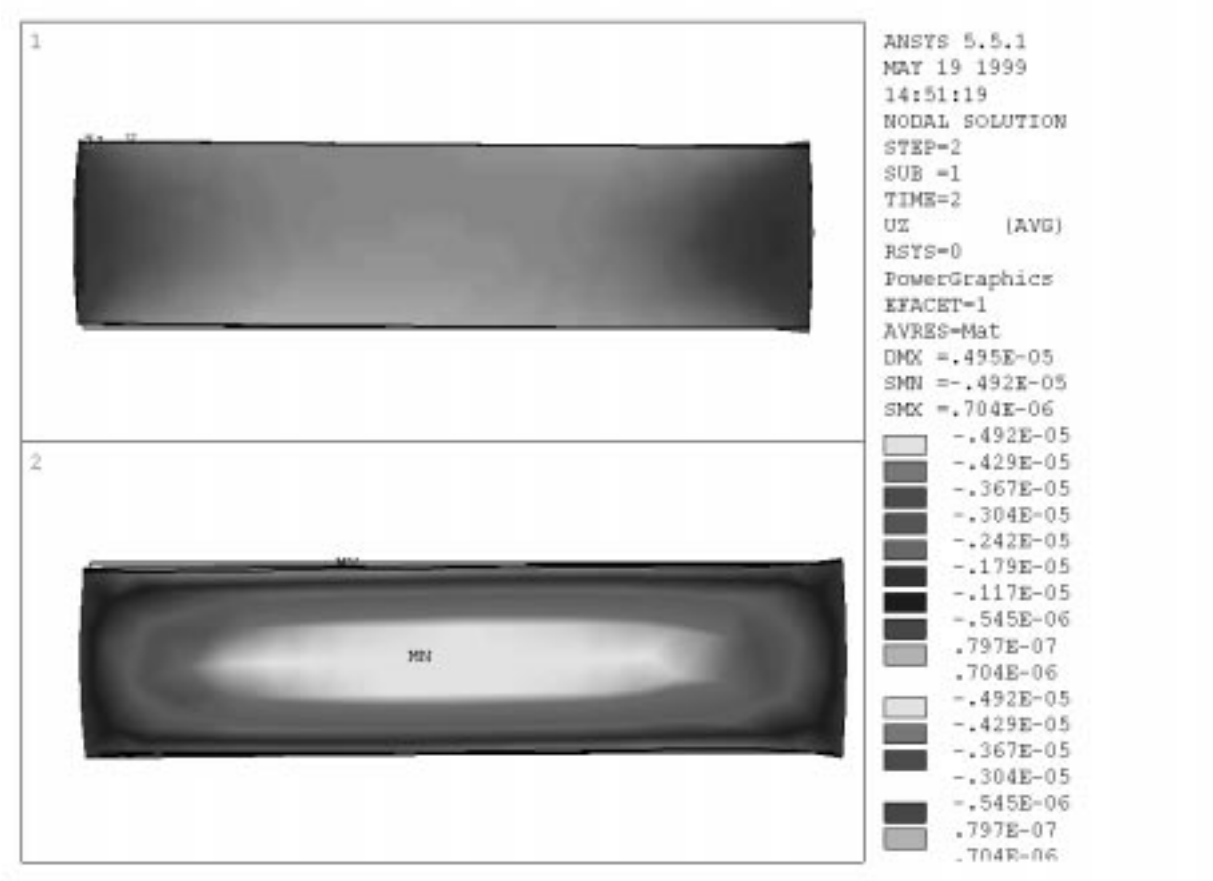

Figure 15: Sandwich cathode X (30 mm thick) deformations due to anode wire stress ($T = 40$ g/wire).

cables from the cathode to the motherboard.

The present calculations with the ANSYS code used a model with homogeneous foam layer without holes. If the hole area is small compared to the total one, the deformations change roughly by the same ratio.

The deformation of the wire-supporting cathode X (thickness=30 mm) due to wire stress ($T =$ 40 g/wire) is illustrated in Figure 15. The sandwich deformations are below 5 microns. Figure 16 demonstrates that the deformation due to wire tension and overpressure at the level of 2 mm of water are still within the tolerances quoted above (see Section 2.3): the maximum deviation for the thin cathode Y is 28 microns and it is 7.5 microns for the thick cathode X. Note that the thickness of the cathode Y could be increased without noticeable increase of the total radiation length.

One should also keep in mind that the holes in Rohacell and in the motherboard would increase the deformations by 15-50 %.

5 Chariot Design.

The general view of the last stations, trigger and muon filter support system (so-called chariot) is presented in Figure 17. Each chamber is attached at points A, B and C to the auxiliary frames **1** and **2** (see Figure 17). It can be moved with respect to these frames along the Z axis (beam direction) and rotated around axis X and Z. One can move independently each half of the frame using the small carriages **3** which simplifies assembling and maintenance. There are two options for chamber displacement (both use the helical gear): 1 – manual drive (in this case one needs access from the top of the chariot); 2 – electric drive.

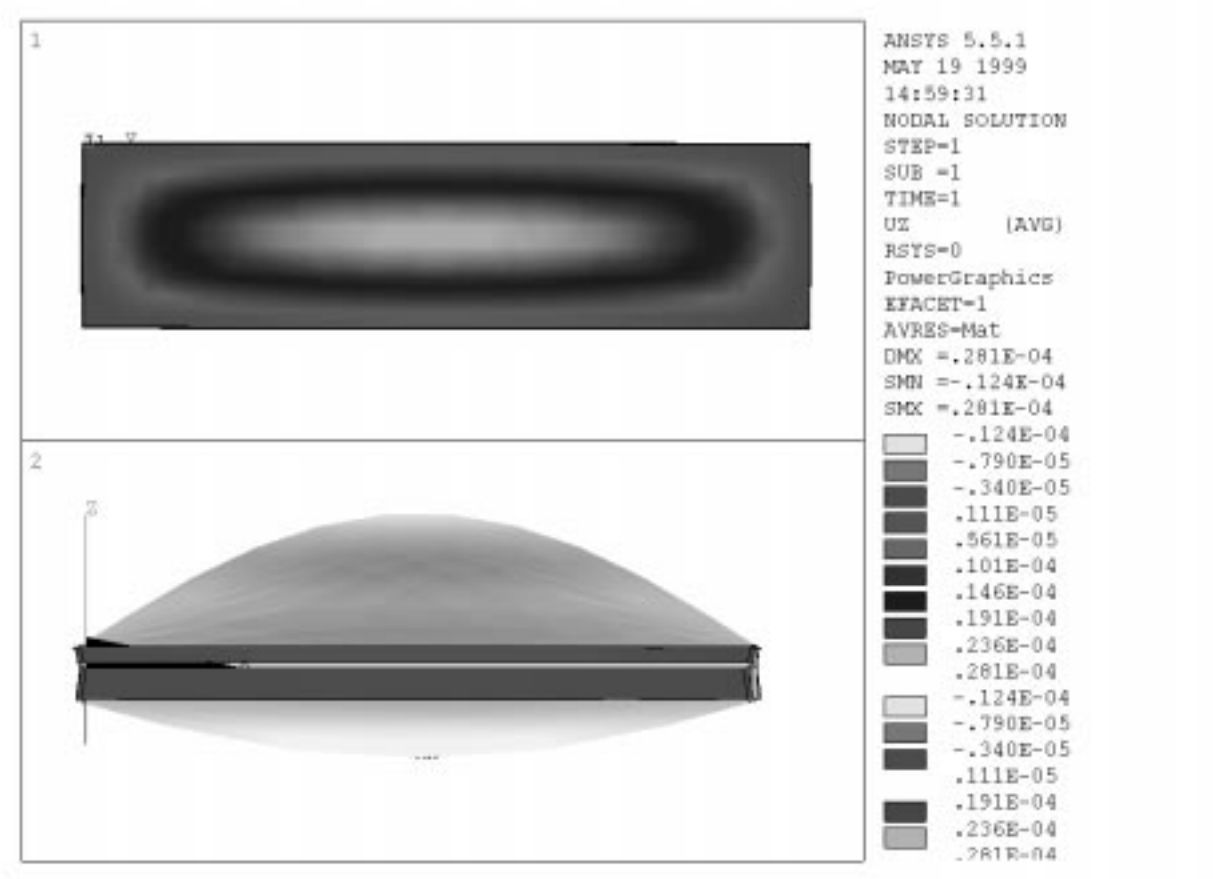

Figure 16: Sandwich cathodes Y deformations due to anode wire stress ($T = 40$ g/wire) and overpressure of 2 mm of water.

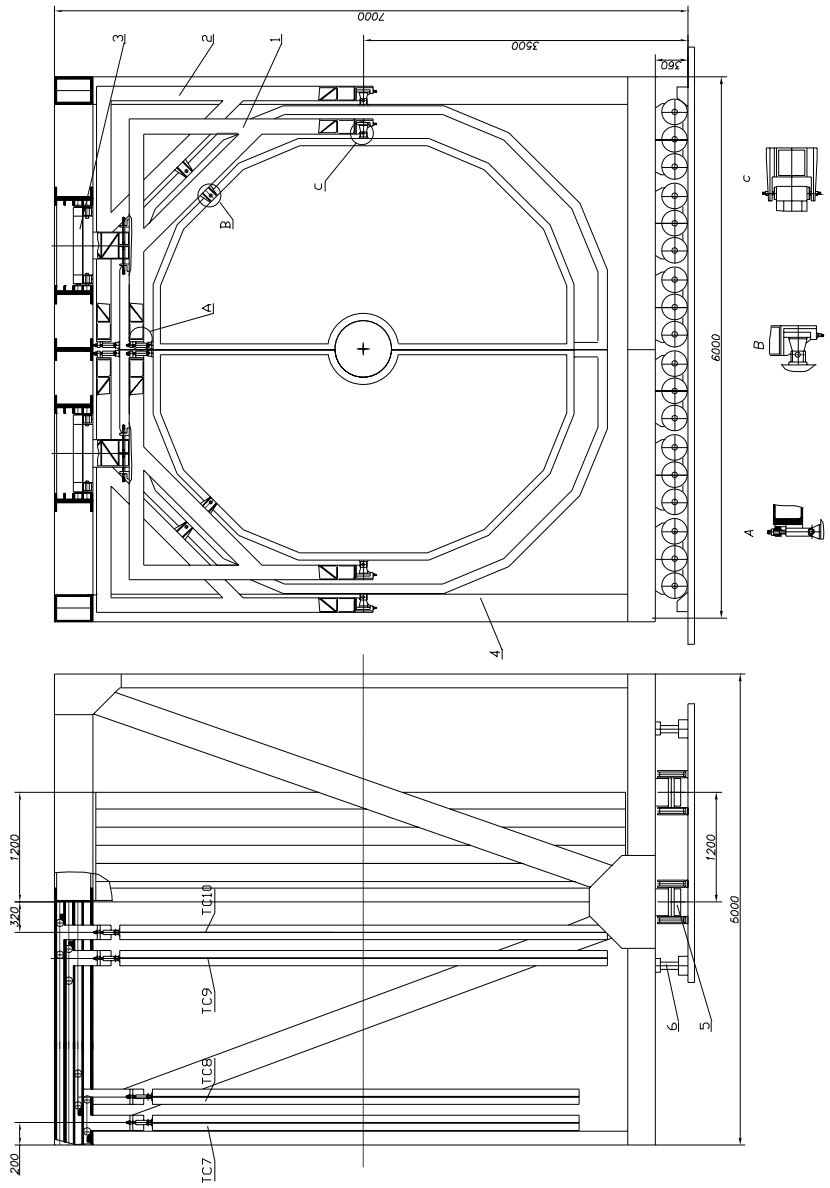

Figure 17: The drawing of the support structure for the last stations. The frame fixation elements at points A, B and C are depicted below.

In one version the muon shield is expected to be a self-supporting structure, independent on the chariot. It is also interesting to consider the muon filter iron as a chariot element, supporting the overall frame (**4**).

The chariot could be moved on four rails using 6 carriages (**5**), each having 6 wheels, 400 mm in diameter. The chariot could be moved using either hydraulics or helical gear or electrical drives.

In order to fix the chariot at utmost position and to have a possibility for adjustment along axis Z one can use hydraulic jacks (**6**) in Figure 17). The force on the jacks is estimated to be at the level of 40 tons.

6 Conclusions.

The above consideration demonstrates the feasibility of a modular approach for the construction of Stations 4 and 5 of the ALICE Muon Spectrometer. We may summarize some positive features of this approach:

- The construction of the modules is based on proven technologies exploited already in several laboratories. It can be realized at PNPI as well as in other laboratories participating in the ALICE muon project.
- The material budget is well within the ALICE TP requirements (less than 3 % of X_0) per chamber layer. Since the modules being are on the external frame, there is no fixation material in the sensitive area of the tracking stations.
- The reliable and straightforward alignment procedure of the modules using both physical particles and reference points.
- The 1-D overlapping in the proposed ladder approach does not create any serious problems in the thickness of the material and in the assembling procedure.
- Easy access to the modules for the replacements of the front-end electronics or the modules.
- Possibility to operate with high density of the read-out electronics distributed over the chamber surface as it was demonstrated in the Orsay and PNPI prototypes.
- Simple gas supply and high and low voltage distribution.
- Possibility to localize and to make reparations of the defective wires.

Acknowledgements.

We like to thank Alexei Vorobyov for his help, interest and valuable suggestions.

Special thanks to Jurgen Schukraft for his constant interest and support of the work.

It is a pleasure to acknowledge here the valuable advises and assistance given to the PNPI team by François Piuz.

We are grateful to our colleagues from IPN Lyon and Orsay for numerous useful discussions.

Kind assistance and patient corrections of the numerous English errors in the text done by Guy Paic are gratefully accepted.

References

[1] *The forward spectrometer of ALICE, Addendum to the Technical Proposal for LHC experiment at CERN*, CERN/LHCC/96-32 LHCC/P3/Addendum 1, 15 October 1996

[2] V. Nikulin and A. Vorobyov, *ALICE di-muon spectrometer. The last stations: possible design.* Internal note/DIM ALICE/96-23.

[3] V. Astashin, V. Gertsenstein, B. Komkov, V. Kozlov, L. Kudin, V. Mylnikov, V. Nikulin, V. Samsonov, G. Shabliy and S. Volkov. *PNPI status report 1998* (presented at the ALICE week in March 1999 (see file ∼/nikulin/public/rep99.ps).

[4] V. Astashin, V. Gertsenstein, B. Komkov, V. Kozlov, L. Kudin, V. Mylnikov, V. Nikulin, V. Samsonov, G. Shabliy, S. Volkov and A. Vorobyov. *PNPI status report 1997* (presented at the ALICE week in November 1997)

[5] V. Gratchev, M. Mohammadi-Baarmand, V. Polychronakos, J. Shank, V. Tcherniatine, A. Vaniachine; *Double track resolution of cathode strip chambers.* NIM **A365** (1995) 576-581.

[6] H. Fenker, J. Thomas, M. Brooks, D. Lea, G. Miller; *Precision Interpolating Pad Chambers.* Proceedings of the 1995 Vienna Wire Chamber Conference, NIM **A367** (1995) 285-289.

[7] V. Nikulin and S. Volkov, *Notes on segmentation of the ALICE muon spectrometer tracking chambers cathodes.* Internal Note/DIM ALICE/99-23.

[8] A. Morsch, private communication. See also *http://home.cern.ch/∼morcsh/Performance.html.*

[9] F. Sauli. *Principles of Operation of Multi Wire proportional chambers.* Preprint CERN 77-09 1977, page 56.

[10] J.C. Armitage, S.P. Beingessner, R.K. Carnegie, E.F. Ritchie and J. Waterhouse. *A study of the effect of methane and carbon dioxide concentration on gas amplification in argon based gas mixtures*; NIM A271 (1988) 588–596.

[11] P. Courtat, D. Charlet, S. Lebon, J.M. Martin, R. Sellem, R. Douet, H. Harroch, L. Bimbot, D. Jouan, L. Kharmandarian, Y. Le Bornec, M. Mac Cormick and N. Willis. *A Full-scale prototype for the tracking chambers of the ALICE muon spectrometer. Part II - Electronics: Preamplifier, Read-out prototype;* Preprint IPNO 99-01.